Dynamic and Inherent B_0 Correction for DTI Using Stimulated Echo Spiral Imaging

Alexandru V. Avram,[1]* Arnaud Guidon,[2,3] Trong-Kha Truong,[3] Chunlei Liu,[3] and Allen W. Song[3]

Purpose: To present a novel technique for high-resolution stimulated echo diffusion tensor imaging with self-navigated interleaved spirals readout trajectories that can inherently and dynamically correct for image artifacts due to spatial and temporal variations in the static magnetic field (B_0) resulting from eddy currents, tissue susceptibilities, subject/physiological motion, and hardware instabilities.

Methods: The Hahn spin echo formed by the first two 90° radiofrequency pulses is balanced to consecutively acquire two additional images with different echo times and generate an inherent field map, while the diffusion-prepared stimulated echo signal remains unaffected. For every diffusion-encoding direction, an intrinsically registered field map is estimated dynamically and used to effectively and inherently correct for off-resonance artifacts in the reconstruction of the corresponding diffusion-weighted image.

Results: After correction with the dynamically acquired field maps, local blurring artifacts are specifically removed from individual stimulated echo diffusion-weighted images and the estimated diffusion tensors have significantly improved spatial accuracy and larger fractional anisotropy.

Conclusion: Combined with the self-navigated interleaved spirals acquisition scheme, our new method provides an integrated high-resolution short-echo time diffusion tensor imaging solution with inherent and dynamic correction for both motion-induced phase errors and off-resonance effects. **Magn Reson Med 71:1044–1053, 2014. © 2013 Wiley Periodicals, Inc.**

Key words: diffusion tensor imaging; stimulated echo; off-resonance correction; eddy current correction; magnetic field inhomogeneities

Spatial accuracy of individual diffusion-weighted images (DWIs) is a fundamental requirement for quantitative diffusion tensor imaging (DTI) analysis (1) of white matter microstructure. Because diffusion tensor models are generally fit on a voxel-by-voxel basis (2), misregistration among individual DWIs with different spatial distortions can lead to signal inconsistencies that bias the microstructural assessment (3), resulting in inaccurate estimates of the fractional anisotropy (FA) and mean apparent diffusion coefficient.

Most commonly, spatial distortions in DWIs are caused by magnetic field inhomogeneities generating off-resonance phase error accumulations during the readout window. In addition to the common static B_0 field nonuniformity, diffusion-weighting direction-dependent and dynamic field perturbations arising from eddy currents induced by the large diffusion-weighting gradients can lead to different local distortions in individual DWIs, which introduce significant errors in the calculation of diffusion metrics. Other sources of magnetic field inhomogeneities further exacerbate this issue. For example, subject or physiological motion (i.e., breathing, pulsation, ventricle motion) can alter the orientation-dependent dipolar interaction of tissue magnetic susceptibilities with the main field, while transient field drifts, mechanical vibrations, and hardware instabilities can generate additional intra-scan variations. Put together, these dynamic off-resonance effects can cause severe image artifacts, especially at high fields and in advanced DWI applications that require long scan durations such as full-brain DTI, q-ball imaging (4), high-angular resolution diffusion imaging (5), myelin water weighted DTI (6), multiple pulsed field gradient diffusion MRI (7), or generalized DTI (8).

A number of approaches have been proposed to address off-resonance distortions in the presence of dynamic field inhomogeneities arising from diffusion direction-dependent eddy currents in DTI. One class of techniques corrects for eddy currents using magnetic field maps measured in a phantom for the same diffusion directions as in the DTI scan (9–11), but requires periodic scans for protocol-specific calibration. Alternatively, images acquired with flipped echo-planar imaging (EPI) phase-encoding directions (12,13) or reversed DW orientations (14) can be used to correct for eddy currents, often at a cost of a longer scan duration. Another class of techniques uses innovative acquisition strategies such as a twice-refocused spin-echo (TRSE) diffusion preparation (15,16) to mitigate eddy currents or parallel imaging (17) to reduce distortions. However, these acquisition-based approaches either require a longer echo time (TE), which decreases signal-to-noise ratio (SNR), and/or provide only incremental reduction of distortions, without directly addressing the underlying sources of artifacts. Most importantly, the majority of these techniques assume that the magnetic field inhomogeneities

[1]Section on Tissue Biophysics and Biomimetics, NICHD, National Institutes of Health, Bethesda, Maryland, USA.

[2]Department of Biomedical Engineering, Pratt School of Engineering, Duke University, Durham, North Carolina, USA.

[3]Brain Imaging and Analysis Center, School of Medicine, Duke University, Durham, North Carolina, USA.

Grant sponsor: National Institutes of Health; Grant numbers: R00EB007182; EB009483; NS075017; EB012586, Grant sponsor: Intramural Research Program of the Eunice Kennedy Shriver National Institute of Child Health and Human Development (NICHD).

*Correspondence to: Alexandru V. Avram, Ph.D., National Institute of Child Health and Human Development (NICHD), National Institutes of Health (NIH), 13 South Dr, Rm 3W16, Bethesda, MD.
E-mail: alexandru.avram@nih.gov

Received 7 November 2012; revised 22 March 2013; accepted 24 March 2013

DOI 10.1002/mrm.24767
Published online 29 April 2013 in Wiley Online Library (wileyonlinelibrary.com).

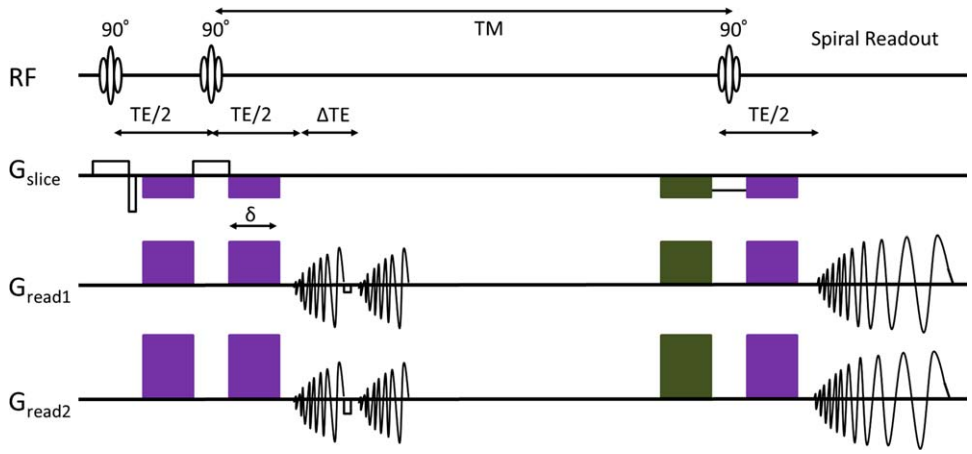

FIG. 1. Pulse sequence diagram for STE spiral DTI with dynamic field map acquisition. The Hahn spin echo pathway formed by the first two 90° RF pulses is refocused using balanced diffusion-weighting gradients (purple) to acquire an inherent field map using two consecutive spiral-out acquisitions at $TE_1 = TE$ and $TE_2 = TE + \Delta TE$. The matching gradient pulses (green) ensure similar eddy currents during the spin echo and STE readouts, and act as crushers for unwanted coherence pathways. [Color figure can be viewed in the online issue, which is available at wileyonlinelibrary.com.]

that are not induced by eddy currents remain constant throughout the scan duration and can be corrected with a separately measured static field map, after image registration. Therefore, even when two or more of these techniques are combined, they cannot correct for off-resonance distortions generated dynamically by sources such as intra-scan variations of B_0 field inhomogeneities, subject/physiological motion, or hardware instabilities. To robustly determine diffusion metrics on a voxel-by-voxel basis, it is necessary to dynamically and inherently correct for off-resonance effects in the presence of both static and dynamic field inhomogeneities in individual DWIs.

On a different front, recent advances in DTI have opened up possibilities to investigate tissue specific characteristics, such as myelin microstructure, which plays a critical role in brain development (6). Because myelin water has a short T_2 of ~25 ms (18), there has been an increasing demand for achieving short TEs in modern DTI. Specifically, the combined use of stimulated echo (STE) and center-out spiral readout trajectories (19) can significantly decrease the TE in DTI experiments, offsetting the 50% decrease in signal compared with spin echo DTI and providing a more sensitive measurement (20). Moreover, STE DTI provides great flexibility with diffusion parameters required for advanced DTI applications (21,22) on clinical scanners, while spiral-out readout trajectories can inherently acquire navigator data enabling multishot imaging with a large imaging matrix size (23). Nevertheless, off-resonance effects during the spiral readout can distort the desired k-space trajectories leading to local blurring, stretching, and shearing in the reconstructed images. The effects of eddy currents in particular can be especially prominent, because the center of k-space is acquired at the beginning of the readout when large eddy currents are generated. While distortion reduction techniques such as TRSE DTI can be extended to STE EPI (20), they do not completely eliminate the eddy current-induced artifacts nor correct for distortions arising from other sources of field inhomogeneities.

Serendipitously, STE spiral DTI does make it possible to develop a unique solution to address both static and dynamic field inhomogeneities in an inherent fashion. In this work, we present an integrated solution for dynamic and inherent off-resonance correction in DTI combining both STE acquisition and self-navigated interleaved spirals (SNAILS) (23). For every diffusion direction, an inherently registered field map is acquired by preserving a secondary Hahn spin echo pathway and subsequently used for off-resonance correction of the corresponding DWI. Taken together, our integrated approach will be able to improve the spatial accuracy of DTI in an inherent and dynamic manner while preserving a short TE. It is hoped that this new methodology will find increased utility in modern DTI applications where spatial accuracy and tissue specificity (e.g., myelin water with short T_2) are critical.

METHODS

Pulse Sequence Design: STE DTI with Dynamic Field Map Acquisition

A multislice STE DTI sequence with SNAILS readout was implemented on a 3 T GE MR750 scanner (Fig. 1). Following a nonspatially selective fat suppression module (not shown in Fig. 1), transverse magnetization is generated with a slice-selective 90° sinc-shaped radiofrequency (RF) pulse. After diffusion encoding, a second 90° RF pulse at TE/2 creates two coherence pathways: the main STE pathway refocused at TM + TE to acquire the desired DWI, and a secondary spin echo pathway formed at TE (24). To mitigate the effect of chemical shift, the third 90° RF pulse is applied with inverted slice selection gradients (25,26). The duration of the longitudinal period (TM) is generally on the order of the tissue T_1 relaxation time constant and can, therefore, be sufficiently long (TM > 100 ms) to allow balancing of the secondary spin echo pathway and acquiring a low-resolution field map.

The STE diffusion signal is measured using a SNAILS center-out readout trajectory. For each shot in the

segmented DTI experiment, the variable-density spiral trajectory (27) oversamples the center of k-space to acquire a low-resolution but full-field of view image, which serves as an inherent navigator to correct for motion-induced random phase errors, as shown previously using spin echo (28). While this acquisition scheme provides high-resolution DTI images with excellent SNR (23), the long readout durations required for self-navigation render the measurement susceptible to off-resonance effects due to static and dynamic field inhomogeneities. To address these limitations, we use a secondary spin echo coherence pathway to acquire additional images and generate inherently registered magnetic field maps.

Specifically, the spin echo pathway formed by the first two 90° RF pulses (24) can be balanced with matching diffusion gradients and acquired at $TE_1 = TE$ using a segmented readout with spiral-out k-space trajectories (Fig. 1). During the time interval TM, the main diffusion-prepared STE pathway stored along the longitudinal axis remains unaffected by any gradient manipulations necessary for the field map acquisition. The amplitude of the secondary Hahn spin echo is 50% of that of a conventional spin echo (refocused using a 180° RF pulse) with the same TE. Because the diffusion pulse durations used in a STE experiment are generally short, the diffusion-weighting on this spin echo pathway is relatively small ($\sim$50 s/mm^2), preserving sufficient signal for the acquisition of a subsequent, asymmetric spin echo at $TE_2 = TE_1 + \Delta TE$ following rephasing of the first readout trajectory (Fig. 1). A dynamic field map is then calculated from the phase difference between the two images. The range of off-resonance frequencies that can be sampled at the Nyquist rate with this strategy depends inversely on ΔTE and is, therefore, restricted by the minimum durations of the readout and the rephasing gradient. Using a segmented spiral trajectory to acquire the two consecutive echoes can drastically reduce ΔTE to values on the order of 3 ms. Finally, to ensure that the spin echo and STE experience similar eddy current effects, an additional and identical gradient lobe (shown in green in Fig. 1) as that used for diffusion-weighting is placed symmetrically to the left of the third 90° RF pulse, resulting in matching gradient pulses preceding both stimulated and spin echoes, while also serving as a crusher gradient to remove any residual magnetization from undesired coherence pathways. As a result, the transient effect of both eddy currents and dynamic tissue susceptibilities on the magnetic field can be accurately mapped and subsequently removed.

Image Acquisition and Processing Strategy for Dynamic and Inherent Off-Resonance Correction

With the newly developed STE-SNAILS pulse sequence, DTI scans were conducted in healthy volunteers who provided informed written consent in compliance with the Institutional Review Board protocol at Duke University Medical Center. Specifically, a set of DTI images were acquired with a matrix size of 192 × 192 over a 24 × 24 cm^2 field of view with a 5 mm slice thickness, TE/TM/pulse repetition time = 22/130/4000 ms, and a b-value of $b = 800$ s/mm^2 applied along 15 noncollinear diffusion orientations. For each image, 8 k-space interleaves were acquired using a variable-density spiral readout trajectory of 29 ms duration with inherent self-navigation capability. On the secondary spin echo pathway, the field map was acquired using segmented variable-density spiral readout trajectory with 8 interleaves, a 5.4 ms readout duration, a 64 × 64 imaging matrix, the same field of view, and $TE_1/TE_2 = 22/27.8$ ms. The total b-value on this pathway was 55 s/mm^2. The inherent field map was calculated from the total phase accumulated during $\Delta TE = 5.8$ ms and used to correct for dynamic off-resonance artifacts in each DWI.

To evaluate the limitations of our technique for correcting a wide range of large field inhomogeneities, the STE SNAILS DTI scan was repeated using linear shimming, a shorter $\Delta TE = 2.8$ ms, and a 52 × 52 imaging matrix for the field map acquisition. To serve as control, a second set of DTI images was acquired using the same scan prescription but with a TRSE DTI pulse sequence with self-compensated eddy currents. To maintain consistency between image artifacts, the same SNAILS acquisition parameters were used for both STE and TRSE DTI scans. For a b-value of 800 s/mm^2, the TRSE SNAILS DTI sequence required a significantly longer TE of $TE_{TRSE} = 60$ ms. The corresponding static field map necessary for off-resonance correction of the TRSE SNAILS DTI data was measured from the phase difference between two images consecutively acquired in separate (spin echo and asymmetric spin echo) scans, using the same shim conditions and readout trajectories as for the dynamic field map measurement in STE DTI, but a ΔTE separation of 1.5 ms. To quantitatively assess the white matter sensitivity of the two methods, temporal SNR maps were computed from nine baseline and diffusion weighted images for both STE and TRSE SNAILS DTI scans.

Spatial eddy current profiles in STE DTI were estimated by subtracting the field map corresponding to the baseline (nondiffusion-weighted) image from those corresponding to the DWIs. The resulting difference maps contained field inhomogeneity contributions with low-spatial frequencies generated by gradient eddy currents and intra-scan variations of tissue magnetic susceptibilities. To remove residual high-spatial frequency noise that might result from imperfect 2D phase unwrapping, or low SNR in regions with large magnetic field inhomogeneities, the difference maps were processed using a 4 × 4 median filter. Finally, the field map corresponding to the baseline image was added back to the filtered eddy current field maps to obtain dynamic and inherent field maps for robust off-resonance correction of individual DWIs.

STE SNAILS DWIs were first reconstructed with phase correction, using the inherent navigator to remove random motion-induced shot-to-shot phase variations in individual interleaves (23,28). To further correct for off-resonance artifacts due to tissue susceptibility- and eddy current-induced magnetic field inhomogeneities, the same images were also reconstructed with simultaneous phase and off-resonance correction (29) based on the inherent magnetic field maps acquired dynamically. The

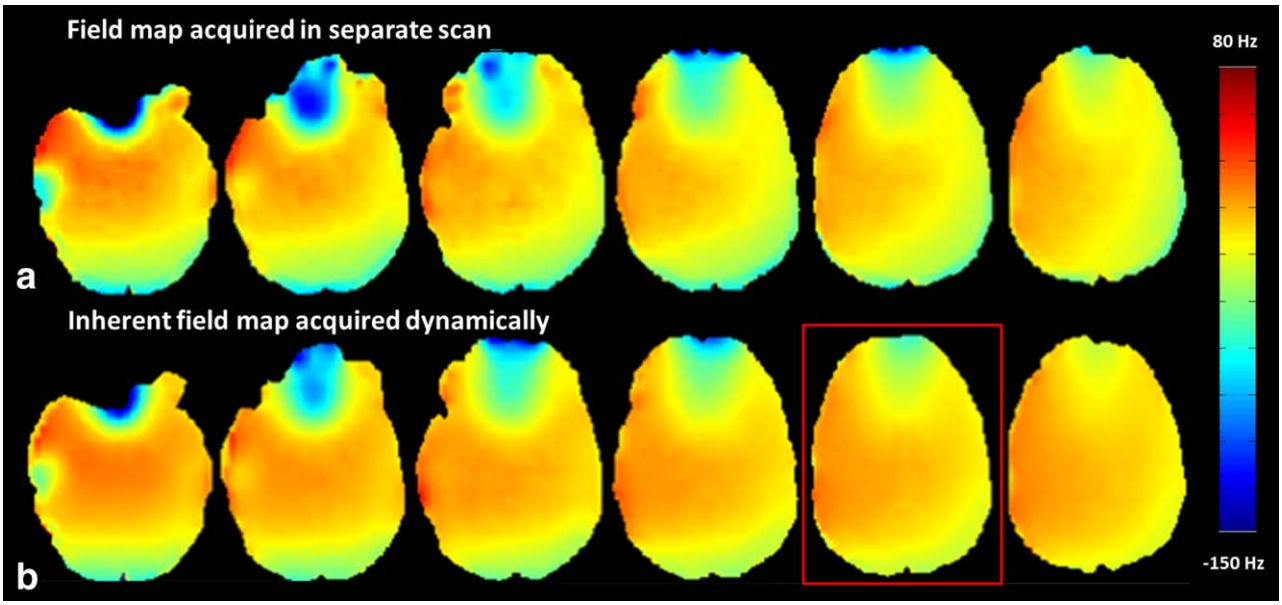

FIG. 2. **a**: Field maps derived from two spiral acquisitions with a 1.5 ms TE separation in six different slices. **b**: Inherent field maps acquired dynamically using the STE DTI sequence with $\Delta TE = 2.8$ ms for the baseline (no diffusion-weighting) images in the same slices. In both experiments, low-resolution field maps were acquired using the same segmented spiral-out readout trajectories and the same linear shim values. Differences between the measured field maps in frontal regions with very large tissue susceptibilities could be caused by subject motion, B_0 drift, or a lower SNR in the STE measurement due to a longer T_2^* decay and an inherent 50% signal reduction. [Color figure can be viewed in the online issue, which is available at wileyonlinelibrary.com.]

raw signals were demodulated at individual frequencies (in increments of 3 Hz) within the range of off-resonance frequencies observed in the field map (−150 Hz to 80 Hz) and subsequently reconstructed using phase correction. The phase corrected images reconstructed at individual demodulation frequencies were then multiplied with corresponding field map-based binary frequency masks before summation (30). The TRSE SNAILS DWIs were reconstructed similarly (both with and without off-resonance correction) by applying the separately acquired field map to all DWIs and compared with the STE SNAILS DWIs reconstructed with dynamic and inherent field map correction. Finally, diffusion tensors were fit to the DTI datasets reconstructed with and without off-resonance correction respectively and measures of FA with principal diffusion direction-encoded color maps were compared quantitatively and qualitatively in white matter regions with highly varying degrees of field inhomogeneities.

RESULTS

To validate the ability of our STE SNAILS DTI method to accurately map magnetic field inhomogeneities using the secondary spin echo pathway, we compared the field maps acquired using STE SNAILS for baseline images (no diffusion-weighting) to field maps derived from separate spin echo scans using the same spiral acquisitions but TEs separated by 1.5 ms. Both field maps revealed frequency shifts in the range of −150 Hz to 80 Hz (Fig. 2). The images generated with both techniques look very similar, even in lower brain slices where large field inhomogeneities are expected. Differences between the two field maps can be attributed to subject motion between scans, B_0 drift, or a lower SNR in the inherently acquired STE field map measurement (due to a longer T_2^* decay and an inherent 50% signal reduction) leading to phase unwrapping errors. This comparison confirms that a wide range of magnetic field inhomogeneities can be accurately mapped using the secondary spin echo pathway in our STE spiral experiment.

Not surprisingly, the inherent field maps acquired dynamically for the baseline image and individual diffusion-weighting directions (Fig. 3a) show clear distinctions depending on the orientation of the applied diffusion-weighting gradients. An estimate of the eddy current maps for each diffusion-weighting direction, including intra-scan variations of other sources of field inhomogeneities, can be obtained by subtracting the field map corresponding to the baseline image from those corresponding to the DWIs (Fig. 3b). As the difference maps reveal, the dynamic contributions from diffusion direction-dependent gradient eddy currents and subject/physiological motion to the off-resonance field varied over a range of 80 Hz in our experiment (Fig. 3b).

For both TRSE-DTI and STE-DTI scans, trapezoidal diffusion gradient pulses with maximum amplitude $G_{max} = 4.9$ G/cm and ramp-up times $r = 1.2$ ms were used to achieve the same diffusion sensitization $b = 800$ s/mm^2 while minimizing TE. For TRSE spiral DTI, a minimum $TE_{TRSE} = 60$ ms was obtained using gradient pulse durations $\delta_1 = \delta_4 = 6.72$ ms and $\delta_2 = \delta_3 = 10.6$ ms, while for STE spiral DTI the minimum TE was reduced to $TE_{STE} = 22$ ms using gradient pulses with durations $\delta = 6.5$ ms separated by $\Delta = 140$ ms. This 63% reduction in TE offsets the inherent 50% signal deficit compared with the TRSE spiral DTI scan and sensitizes the STE spiral DTI experiment to water components with short

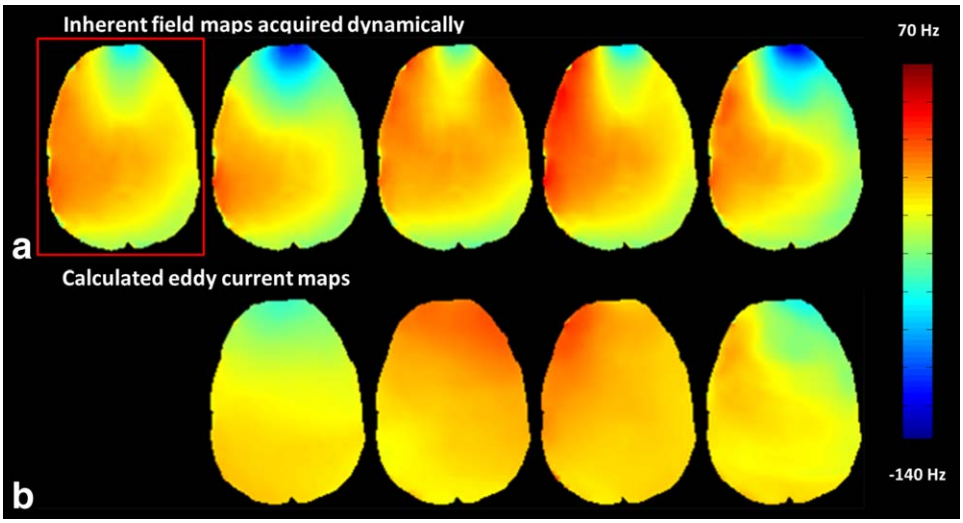

FIG. 3. Variations in maps of magnetic field inhomogeneities acquired dynamically during the STE DTI scan with $\Delta TE = 2.8$ ms. **a**: Field maps acquired dynamically for the baseline image (red box) and four DWIs with different diffusion-weighting orientations during the same STE spiral DTI scan as in Figure 2b. **b**: Corresponding eddy current profiles calculated by subtracting the field map of the baseline image from those of the DWIs in (a). The difference maps indicate that temporal field map variations on the order of 80 Hz occurred during the STE DTI scan. [Color figure can be viewed in the online issue, which is available at wileyonlinelibrary.com.]

T_2 relaxation time constants. Specifically, the 50% signal deficit is reduced to 1.4% assuming a T_2 relaxation time constant of 56 ms for in vivo white matter at 3 T (31) and negligible contributions from longitudinal T_1 relaxation and imperfect RF pulses. To quantify the white matter sensitivity of the proposed method, temporal SNR maps (Fig. 4, bottom row) were computed as the ratio of the mean to the standard deviation of the voxel signal across nine averages for both STE SNAILS DTI (Fig. 4a—baseline, Fig. 4c—diffusion weighted) and TRSE SNAILS DTI (Fig. 4b—baseline, Fig. 4d—diffusion weighted) experiments, following motion and off-resonance correction. In the baseline images, temporal SNR values averaged across a white matter region of interest in the baseline images were 36.1 for TRSE SNAILS DTI and 34.3 for STE SNAILS DTI, in good agreement with the aforementioned theoretical estimations.

We can further calculate a break-even relaxation time $T_{2,be} = 55$ ms for which the signal increase due to the TE reduction compensates for the inherent 50% signal deficit in STE spiral DTI relative to the signal level in TRSE spiral DTI. The STE DTI preparation is expected to preserve more signal from water components with magnetic relaxation time constants $T_2 < T_{2,be} = 55$ ms. The comparison between the STE and TRSE SNAILS baseline images reveals a visibly less pronounced T_2 contrast in the STE acquisition, which has an almost three times shorter TE (Fig. 4a,b). Figure 5 shows the relative signal fractions of water components with T_2 values in the 10–50 ms range calculated for three different diffusion pulse sequences: STE and TRSE spiral DTI and the clinical TRSE DTI with EPI readout, which requires a minimum TE = 86 ms to achieve the same diffusion sensitization of $b = 800$ s/mm^2. With a relaxation time constant of $T_{2,my} = 25$ ms for myelin water (18), we can calculate that in the STE spiral DTI experiment (TE = 22 ms) 21% of the signal from this component is preserved, compared with 9% in the TRSE spiral DTI scan (TE = 60 ms) and only 3% in the standard clinical TRSE DTI with EPI readout (TE = 86 ms), respectively. White matter tissue components with short T_2 relaxation time constants, such as myelin water are virtually undetectable in clinical TRSE DTI EPI experiments with TE > 80 ms, but can be studied using STE spiral DTI.

Figure 6 compares spatial distortions in a low brain slice for STE and TRSE DWIs acquired with linear shimming and reconstructed using different correction methods. In the presence of diffusion sensitization, small subject and physiological motion induced shot-to-shot nonlinear phase variations, resulting in significant signal cancellation in the direct reconstruction of individual STE DWIs by gridding and inverse Fourier transform (Fig. 6a). After phase correction of each interleaf with the inherent navigator data, uniform signal is restored in both STE and TRSE SNAILS DWIs (Fig. 6b,d). As expected, even for the long diffusion times (~150 ms) used in STE experiments, the motion-induced phase in each shot could be successfully removed to yield high-resolution DWIs without the signal loss artifacts commonly seen in multishot diffusion imaging. Finally, after reconstruction using the inherently acquired field map, the spatial accuracy in the STE SNAILS DWI is visibly improved and the diffusion contrast is more localized to individual fibers (Fig. 6c, red box). The final image is comparable with that obtained with TRSE SNAILS DWI after both phase correction and off-resonance correction with a separately acquired field map (Fig. 6e). These results demonstrate that the dynamic field maps acquired with our technique can be used to effectively correct off-resonance artifacts in the corresponding DWIs.

The importance of correcting for dynamic changes in field inhomogeneities (Fig. 3b), i.e., due to eddy currents, tissue susceptibilities, B_0 drifts, etc. can be

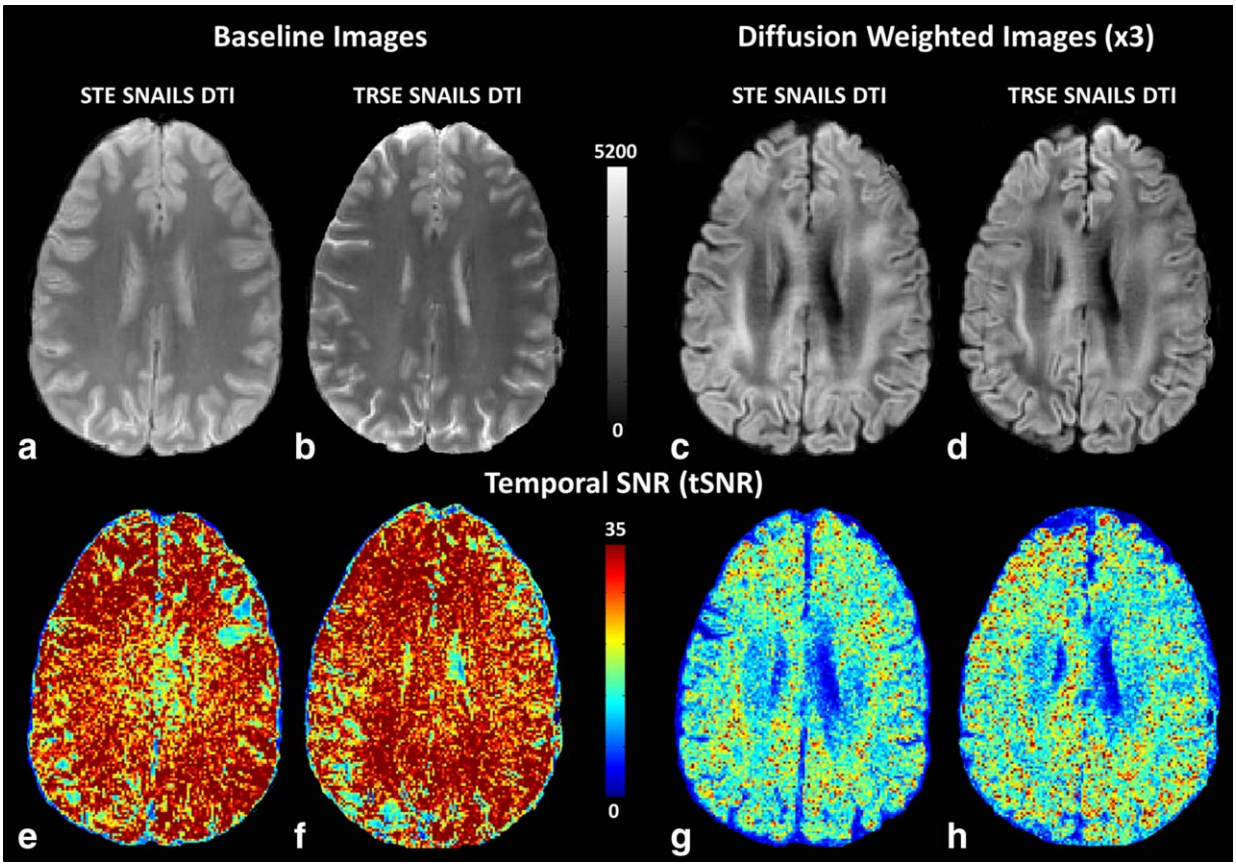

FIG. 4. Top row: Baseline (**a**) and diffusion-weighted (**c**) images measured using the STE SNAILS DTI pulse sequence ($TE_{STE} = 22$ ms) after motion and off-resonance correction using the inherently acquired field maps with $\Delta TE = 2.8$ ms. Baseline (**b**) and diffusion-weighted (**d**) images measured in the same scan session using the TRSE SNAILS DTI pulse sequence ($TE_{TRSE} = 60$ ms) after motion and off-resonance correction using a separately acquired field maps with $\Delta TE = 1.5$ ms. Differences in tissue contrast reflect the significantly shorter TE achieved with STE SANILS DTI. For both scans, the same linear shimming parameters were used. Bottom row: Temporal SNR maps calculated using nine averages for the images on the top row. The similar temporal SNR values agree well with the theoretical predictions and confirm that for white matter the short TE obtained with the STE DTI preparation offsets the 50% signal deficit relative to the signal level in the TRSE DTI experiment. [Color figure can be viewed in the online issue, which is available at wileyonlinelibrary.com.]

appreciated in Figure 7. Phase corrected STE DWIs show different amounts of local blurring and stretching depending mainly on the orientation of the applied diffusion-weighting gradients (Fig. 7a,c,e). In particular, gray matter signal from sulci and gyri is distributed to the neighboring voxels, leading to erroneous measurements in adjacent white matter tracts (Fig. 7, arrows). After off-resonance correction with inherent field maps, various local blurring artifacts are specifically removed in both the baseline image and individual DWIs leading to a greatly improved spatial accuracy (Fig. 7b,d,f). These results illustrate the ability of our methodology to distinctively remove off-resonance artifacts in each DWI and underline the necessity for such a correction.

Finally, diffusion tensors were fit to the STE SNAILS DTI dataset and the FA modulated diffusion direction-encoded color maps were compared before (Fig. 8a–c) and after off-resonance correction (Fig. 8d–f). As expected, due to direction-dependent image blurring, the uncorrected images have vaguely delineated white matter features and reduced FA values in the white matter fibers affected by field inhomogeneities, especially by eddy currents. After correction, the FA maps are

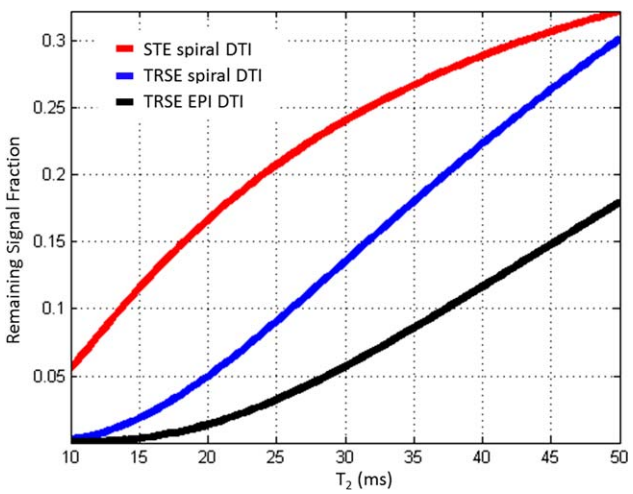

FIG. 5. Baseline signal fractions of water components with short T_2 relaxation time constants for three MRI diffusion pulse sequences with $b = 800$ s/mm^2 and minimum echo times: STE spiral DTI (TE = 22 ms), TRSE spiral DTI (TE = 60 ms), and the clinical TRSE EPI DTI (TE = 86 ms) sequence, respectively. [Color figure can be viewed in the online issue, which is available at wileyonlinelibrary.com.]

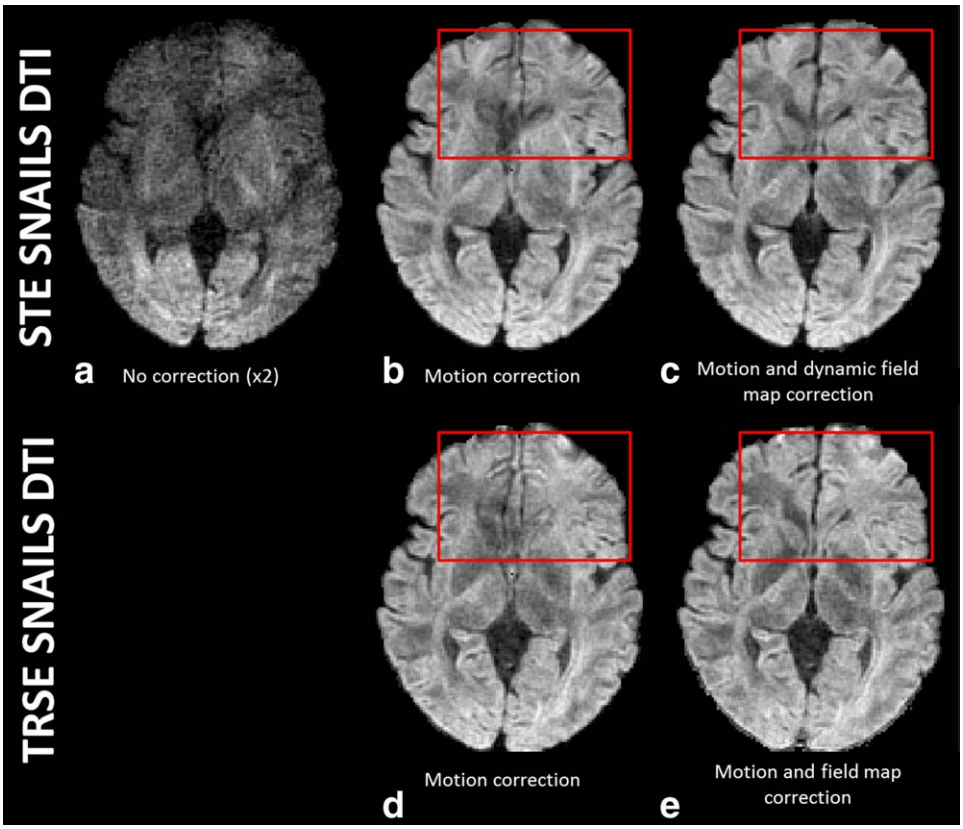

FIG. 6. Integrated motion and dynamic field map correction in STE SNAILS DTI. Top row: STE SNAILS diffusion-weighted image in a low brain slice acquired with linear shimming and $\Delta TE = 2.8$ ms. The intensity variation in the magnitude image reconstructed using direct gridding of individual interleaves followed by Fourier inversion (**a**) can be removed with phase correction using the inherently acquired navigator signals (**b**). However, the motion corrected images show significant image blurring due to field inhomogeneities, especially in the frontal brain regions (b, red box). After off-resonance correction using the dynamically acquired field map, spatial accuracy is restored and the final image (**c**) is comparable with that acquired with TRSE SNAILS DTI (bottom row) and corrected for motion (**d**) and off-resonance effects using a separately acquired field map (**e**). [Color figure can be viewed in the online issue, which is available at wileyonlinelibrary.com.]

significantly improved and small white matter fibers in the posterior and anterior regions become considerably more discernible and localized (Fig. 8, arrows). To quantitatively assess the improvements in FA, the average FA was measured in three white matter regions of interest (splenium and genu of the corpus callosum, and corticospinal tract) for both DTI datasets reconstructed with and without dynamic field map correction (Table 1). As expected, noncorrected images revealed low FA values that varied significantly across the three regions of interest: 0.54 in the genu of the corpus callosum compared with 0.68 in the splenium of the corpus callosum and 0.59 in the corticospinal tract. After dynamic field map correction of the STE-DTI dataset, FA maps showed improved spatial accuracy and larger, consistent values: 0.70 in the genu and splenium of the corpus callosum, and 0.63 in the corticospinal tract. Minor inconsistencies between FA values measured in the corrected STE SNAILS DTI and TRSE SNAILS DTI datasets could be due to different signal weightings of white matter T_2 components caused by the different TEs of the two experiments ($TE_{STE} = 22$ ms and $TE_{TRSE} = 60$ ms) and partial volume averaging effects caused by subject motion.

DISCUSSIONS AND CONCLUSION

It is generally known that, even with advanced shimming methods, spatially and temporally varying magnetic field inhomogeneities due to gradient eddy currents, intra-scan B_0 field variations, subject/physiological motion, or hardware instabilities, can generate dynamic off-resonance effects during DTI scans. The resultant phase errors accumulated during the readout period distort the reconstructed DWIs and introduce severe errors in the quantitative estimation of the diffusion tensors. Among the numerous approaches proposed for off-resonance correction in DTI, many come at the cost of longer scan duration, additional calibration scans, or extra hardware and can be well-suited for specific applications. For example, the reversed-DW orientation method (14) may not double scan time if a full q-ball shell (4) or diffusion spectrum imaging lattice (32) is acquired, but can only correct for field inhomogeneities caused by eddy currents. The flipped EPI phase-encoding direction technique (12,13) can correct for both eddy current- and tissue susceptibility-induced field inhomogeneities dynamically, provided that images with reversed phase-encoding directions are acquired

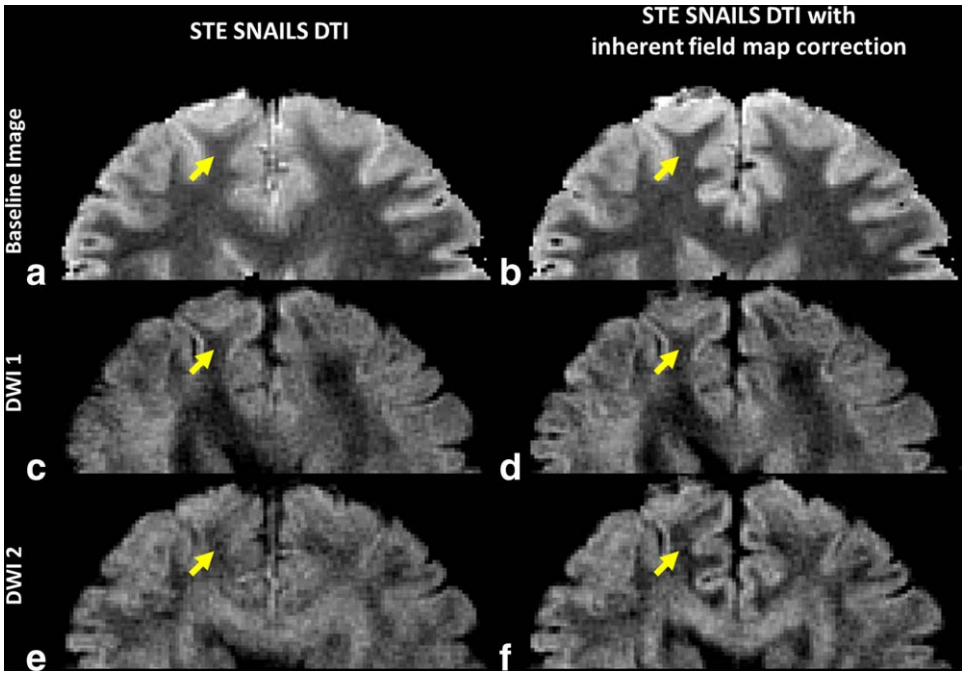

FIG. 7. Specific correction of individual DWIs using dynamically acquired inherent field maps. Left: STE spiral baseline (nondiffusion-weighted) and DW images reconstructed with phase correction only. Right: The same images reconstructed with simultaneous phase and off-resonance correction using the field map acquired dynamically with the STE SNAILS DTI pulse sequence. Due to gradient eddy currents, the same white matter fiber (e.g., yellow arrow) experiences different amounts of local blurring for different diffusion orientations (**c**—moderate, **e**—severe). After off-resonance correction using the inherent field maps acquired dynamically, these image artifacts are specifically removed (**d** and **f**). Similarly, in the baseline image (**a**), the tissue susceptibility-induced local blurring artifacts are effectively removed (**b**). Note the overall improvement in image clarity in the right column. Dynamic field maps were acquired with $\Delta TE = 5.8$ ms and high-order polynomial shimming of the magnetic field. [Color figure can be viewed in the online issue, which is available at wileyonlinelibrary.com.]

consecutively to minimize registration errors. However, the Cartesian k-space trajectory that enables this correction scheme requires a long TE in diffusion imaging, providing limited sensitivity, especially to short-T_2 tissue water components (Fig. 5), and restricting the maximum imaging matrix size. In comparison, our newly developed STE-DTI method can be used with arbitrary readout trajectories (i.e., to minimize TE) and offers an integrated and inherent solution to correct for artifacts arising from both static and dynamic field inhomogeneities without additional scans or hardware.

In theory, the dynamic and inherent field map acquisition can be designed independently from that of the DWIs, using different spatial and temporal resolutions. However, for full brain applications, the field map acquisition should use the same number of interleaves as the DTI acquisition and a minimal readout duration. Both the range of magnetic field inhomogeneities that can be corrected using this technique and the spatial resolution of the field maps are limited by the TE separation (ΔTE) between the two consecutive spin echo readouts. As shown in Figure 3, a ΔTE of 3 ms can be used to correct for a wide range of off-resonance frequencies in the entire brain using an attainable resolution of 52×52 for field maps with high SNR. Because dynamic magnetic field inhomogeneities due to tissue susceptibilities, eddy currents, subject/physiological motion, and hardware instabilities exhibit smooth spatial variations, low-resolution field maps are generally sufficient for off-resonance correction and can be acquired with a short ΔTE. On the contrary, when longer ΔTE durations are used to acquire high-resolution field maps, off-resonance effects in regions with large magnetic susceptibility differences between adjacent tissues can result in a reduced sensitivity due to T_2^* dephasing and considerable phase unwrapping errors, especially at high field. In this case, high-order polynomial shimming of the static magnetic field should be concurrently used to reduce the range of off-resonance effects and allow imaging in ventral brain regions. Finally, it should be noted that although our implementation uses a spiral trajectory to achieve a short TE, the proposed inherent and dynamic field mapping methodology is compatible with other fast imaging readout trajectories such as single-shot EPI, segmented EPI, or PROPELLER EPI (33) and can be integrated with parallel imaging to reduce the total scan time.

It is also worth mentioning that the diffusion direction-dependent eddy currents (in the range of 80 Hz at 3 T) are generally modeled as multiexponential decays, with time constants ranging up to 100 ms. When compared with TRSE DTI, the significantly shorter diffusion pulses ($\delta < 10$ ms) and small gradient duty cycles in our STE DTI generate lower eddy current levels and smaller contributions from eddy current components with long time constants. In cases when center-out k-space trajectories (such as those used in the SNAILS acquisition) are

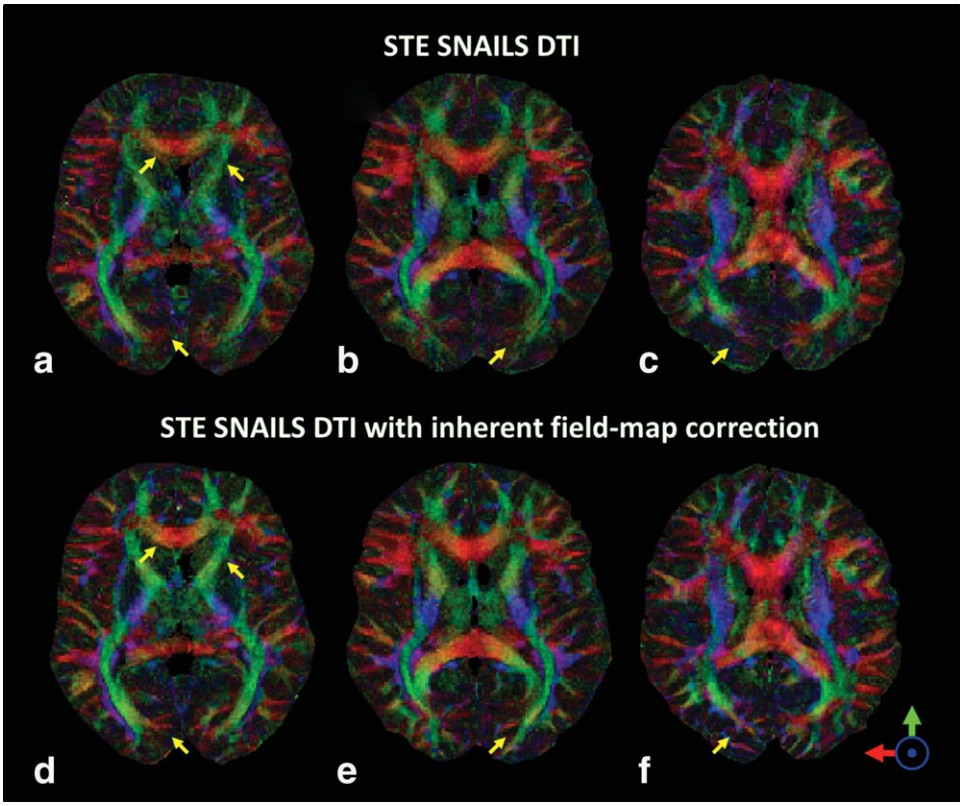

FIG. 8. Restored spatial accuracy in STE SNAILS DTI after off-resonance correction with inherently acquired field maps. Top row: Fractional anisotropy (FA) maps with principal diffusion orientation color coding for three slices reconstructed with phase correction only. Bottom row: Corresponding directionally encoded color FA images after simultaneous phase and off-resonance correction with inherently acquired field maps. After correction, the FA maps are improved and small white matter fibers (arrows) become significantly more localized and discernible. Dynamic field maps were acquired with $\Delta TE = 5.8$ ms and high-order polynomial shimming of the magnetic field.

used to minimize TE and increase the SNR, the eddy current components with short and medium time constants generated by the proximate diffusion pulse can significantly distort the reconstructed image. Steidle and Schick proposed an eddy current suppression method for STE diffusion MRI with EPI acquisition similar to TRSE DTI (34), with bipolar compensation gradient pulses applied during the TM period (20). While their technique successfully mitigates slowly decaying eddy current contributions, it has limited efficacy for suppressing eddy current components with short time constants on the order of the diffusion pulse duration δ ($\sim$10 ms), which dominate in STE DTI, especially when center-out readout trajectories are used to minimize TE. Most importantly, similarly to the TRSE DTI method, the solution proposed by Steidle and Schick does not completely correct for either static or dynamic eddy currents and magnetic field variations. The advantage of our approach is that all field maps are acquired inherently and can effectively measure both the slow and the dominant fast decaying eddy current components. Moreover, unlike TRSE-based methods, which require registration with a separately acquired field map to correct for static B_0 field inhomogeneities, our technique corrects for both static and dynamic field inhomogeneities using intrinsically registered field maps measured on a secondary spin-echo coherence pathway generated by the same RF pulses as the DW STE signal.

In our experiment, the TE for both the STE and the spin echo (used for field map estimation) was 22 ms, but the b-value on the main STE pathway ($b_{STE} = 800$ s/mm^2) was an order of magnitude larger than on the spin echo pathway ($b_{SE} = 55$ s/mm^2), resulting in a $q = 136$ cm^{-1}. Due to the long mixing period (TM = 130 ms) in STE diffusion MRI, this relative proportion between the b-values is maintained even if longer diffusion gradient pulse durations δ are used to obtain higher q-values. Therefore, the signal loss due to diffusion attenuation on the secondary spin echo pathway does not limit the proposed STE-DTI method to small q-values. Nevertheless, for very large diffusion gradient pulse durations, the amount of diffusion sensitization on the spin echo pathway could lead to motion-induced phase inconsistencies in the multishot acquisition potentially deteriorating the reliability of the field map calculation. In general, however, the STE diffusion experiment uses short diffusion gradient pulse durations δ to minimize TE and is, therefore, uniquely suited for myelin water diffusion MRI (6) and advanced diffusion models such as CHARMED (21)

Table 1
Quantitative Region of Interest-Based Analysis of Fractional Anisotropy Measured Using STE SNAILS DTI with and without Dynamic Field Map Correction and TRSE SNAILS DTI with Field Map Correction (w/fm) in Fibers Along the Genu and Splenium of the Corpus Callosum (CC) and the Corticospinal Tract

	STE SNAILS DTI	STE SNAILS DTI (w/fm)	TRSE SNAILS DTI (w/fm)
Genu of the CC	0.54	0.70	0.75
Splenium of the CC	0.68	0.70	0.73
Corticospinal tract	0.59	0.63	0.60

or AxCaliber (22), which rely on the validity of the short gradient pulse-width approximation $\delta \rightarrow 0$.

Furthermore, when compared with a conventional TRSE DTI EPI sequence (which is the current standard acquisition protocol for clinical DTI), the inherent half signal reduction in our STE-DTI method can be advantageously offset by a greatly shortened TE for the same diffusion weighting (20). The spiral-out readout trajectory further minimizes the achievable TE, providing an excellent sensitivity especially for tissues with short T_2-relaxation times such as white matter or myelin water (Fig. 5). The exclusive use of short TEs for in vivo DTI could help reveal unique information about myelin microstructural changes during early development or pathology (6).

In summary, we have shown in this report that a STE acquisition can be effectively combined with a SNAILS readout (23) to achieve very short TEs and high SNRs, preserving the sensitivity to short-T_2 tissues. Furthermore, we have demonstrated that our inherently navigated acquisition strategy can reliably remove dynamic phase errors in different diffusion directions that are otherwise difficult to correct. Thus, our current implementation provides an integrated solution for high-resolution short-TE DTI with inherent motion and off-resonance correction capabilities. Given the increasing utility of advanced DTI methods in the clinical settings, this integrated and robust method could potentially find a wide range of in vivo applications in brain and body MRI where high spatial fidelity and resolution are required.

ACKNOWLEDGMENTS

This work was supported in part by the Intramural Research Program of the Eunice Kennedy Shriver National Institute for Child Health and Human Development within the National Institutes of Health. A.V.A. was also supported by the Intramural Research Program of the *Eunice Kennedy Shriver* National Institute of Child Health and Human Development (NICHD). The authors also thank Dr. Nan-Kuei Chen for helpful discussions.

REFERENCES

1. Basser PJ, Mattiello J, LeBihan D. MR diffusion tensor spectroscopy and imaging. Biophys J 1994;66:259–267.
2. Basser PJ, Pierpaoli C. A simplified method to measure the diffusion tensor from seven MR images. Magn Reson Med 1998;39:928–934.
3. Pierpaoli C, Basser PJ. Toward a quantitative assessment of diffusion anisotropy. Magn Reson Med 1996;36:893–906.
4. Tuch DS. Q-ball imaging. Magn Reson Med 2004;52:1358–1372.
5. Frank LR. Anisotropy in high angular resolution diffusion-weighted MRI. Magn Reson Med 2001;45:935–939.
6. Avram AV, Guidon A, Song AW. Myelin water weighted diffusion tensor imaging. Neuroimage 2010;53:132–138.
7. Avram AV, Özarslan E, Sarlls JE, Basser PJ. In vivo detection of microscopic anisotropy using quadruple pulsed-field gradient (qPFG) diffusion MRI on a clinical scanner. Neuroimage 2013;64:229–239.
8. Liu C, Mang SC, Moseley ME. In vivo generalized diffusion tensor imaging (GDTI) using higher-order tensors (HOT). Magn Reson Med 2010;63:243–252.
9. Truong TK, Chen B, Song AW. Integrated SENSE DTI with correction of susceptibility- and eddy current-induced geometric distortions. Neuroimage 2008;40:53–58.
10. Chen B, Guo H, Song AW. Correction for direction-dependent distortions in diffusion tensor imaging using matched magnetic field maps. Neuroimage 2006;30:121–129.
11. Truong TK, Chen NK, Song AW. Dynamic correction of artifacts due to susceptibility effects and time-varying eddy currents in diffusion tensor imaging. Neuroimage 2011;57:1343–1347.
12. Gallichan D, Andersson JLR, Jenkinson M, Robson MD, Miller KL. Reducing distortions in diffusion-weighted echo planar imaging with a dual-echo blip-reversed sequence. Magn Reson Med 2010;64:382–390.
13. Embleton KV, Haroon HA, Morris DM, Ralph MAL, Parker GJM. Distortion correction for diffusion-weighted MRI tractography and fMRI in the temporal lobes. Hum Brain Mapp 2010;31:1570–1587.
14. Bodammer N, Kaufmann J, Kanowski M, Tempelmann C. Eddy current correction in diffusion-weighted imaging using pairs of images acquired with opposite diffusion gradient polarity. Magn Reson Med 2004;51:188–193.
15. Reese TG, Heid O, Weisskoff RM, Wedeen VJ. Reduction of eddy-current-induced distortion in diffusion MRI using a twice-refocused spin echo. Magn Reson Med 2003;49:177–182.
16. Finsterbusch J. Double-spin-echo diffusion weighting with a modified eddy current adjustment. Magn Reson Imaging 2010;28:434–440.
17. Pruessmann KP, Weiger M, Scheidegger MB, Boesiger P. SENSE: sensitivity encoding for fast MRI. Magn Reson Med 1999;42:952–962.
18. Mackay A, Whittall K, Adler J, Li D, Paty D, Graeb D. In vivo visualization of myelin water in brain by magnetic resonance. Magn Reson Med 1994;31:673–677.
19. Frank LR, Wong EC, Liu TT, Buxton RB. Increased diffusion sensitivity with hyperechos. Magn Reson Med 2003;49:1098–1105.
20. Steidle G, Schick F. Echoplanar diffusion tensor imaging of the lower leg musculature using eddy current nulled stimulated echo preparation. Magn Reson Med 2006;55:541–548.
21. Assaf Y, Basser PJ. Composite hindered and restricted model of diffusion (CHARMED) MR imaging of the human brain. Neuroimage 2005;27:48–58.
22. Assaf Y, Blumenfeld-Katzir T, Yovel Y, Basser PJ. AxCaliber: a method for measuring axon diameter distribution from diffusion MRI. Magn Reson Med 2008;59:1347–1354.
23. Liu C, Bammer R, Kim DH, Moseley ME. Self-navigated interleaved spiral (SNAILS): application to high-resolution diffusion tensor imaging. Magn Reson Med 2004;52:1388–1396.
24. Hahn EL. Spin echoes. Phys Rev 1950;80:580–594.
25. Sarlls JE, Pierpaoli C, Talagala SL, Luh W-M. Robust fat suppression at 3 T in high-resolution diffusion-weighted single-shot echo-planar imaging of human brain. Magn Reson Med 2011;66:1658–1665.
26. Gomori JM, Holland GA, Grossman RI, Gefter WB, Lenkinski RE. Fat suppression by section-select gradient reversal on spin-echo MR imaging. Work in progress. Radiology 1988;168:493–495.
27. Kim D-H, Adalsteinsson E, Spielman DM. Simple analytic variable density spiral design. Magn Reson Med 2003;50:214–219.
28. Miller KL, Pauly JM. Nonlinear phase correction for navigated diffusion imaging. Magn Reson Med 2003;50:343–353.
29. Liu C, Moseley ME, Bammer R. Simultaneous off-resonance and phase correction for multi-shot DWI. In Proceedings of the 13th Annual Meeting of ISMRM, Miami, Florida, USA, 2005. p. 5.
30. Noll DC, Pauly JM, Meyer CH, Nishimura DG, Macovski A. Deblurring for non-2D Fourier transform magnetic resonance imaging. Magn Reson Med 1992;25:319–333.
31. Gelman N, Gorell JM, Barker PB, Savage RM, Spickler EM, Windham JP, Knight RA. MR imaging of human brain at 3.0 T: preliminary report on transverse relaxation rates and relation to estimated iron content. Radiology 1999;210:759–767.
32. Wedeen VJ, Hagmann P, Tseng W-YI, Reese TG, Weisskoff RM. Mapping complex tissue architecture with diffusion spectrum magnetic resonance imaging. Magn Reson Med 2005;54:1377–1386.
33. Pipe JG, Farthing VG, Forbes KP. Multishot diffusion-weighted FSE using PROPELLER MRI. Magn Reson Med 2002;47:42–52.
34. Reese TG, Heid O, Weisskoff RM, Wedeen VJ. Reduction of eddy-current-induced distortion in diffusion MRI using a twice-refocused spin echo. Magn Reson Med 2003;49:177–182.